BIOCHEMISTRY
including biophysical chemistry & molecular biology

Article

pubs.acs.org/biochemistry

Identification of Tyr241 as a Key Catalytic Base in the Family 4 Glycoside Hydrolase BglT from *Thermotoga maritima*

Vivian L. Y. Yip and Stephen G. Withers*

2036 Main Mall, Department of Chemistry, University of British Columbia, Vancouver, BC, Canada V6T 1Z1

ABSTRACT: While the vast majority of glycosidases catalyze glycoside hydrolysis via oxocarbenium ion-like transition states and typically employ carboxylic acid residues as acid/base or nucleophile catalysts, two subfamilies of these enzymes (GH4 and GH109 in the CAZY classification) conduct hydrolysis via a redox-assisted mechanism involving anionic transition states. While good evidence of this mechanism has been obtained, the identities of the catalytic residues involved have not yet been confirmed. Mechanistic analyses of mutants of the 6-phospho-β-glucosidase from *Thermotoga maritima* (BglT), in which the active site tyrosine residue (Tyr 241) has been replaced with Phe and Ala, provide support for its role as a catalytic base. The pH dependence of k_{cat} and k_{cat}/K_m, particularly of the acidic limb corresponding to the base, is shifted relative to that of the wild-type enzyme. Kinetic isotope effects for hydrolysis of substrates deuterated at C1, C2, and C3 by the Tyr 241 mutants are strongly pH-dependent, with essentially full primary kinetic isotope effects being observed for the 2-deutero substrate at low pH with the Tyr241Ala mutant. This is consistent with a slowing of the deprotonation step upon removal of the base.

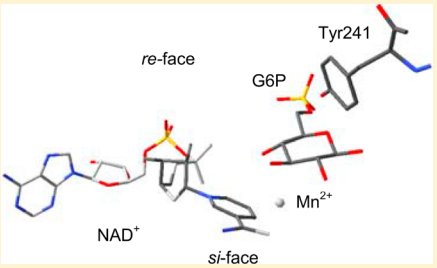

Glycosidases represent a large family of enzymes responsible for the hydrolytic cleavage of glycosidic bonds in a variety of contexts. They have been grouped into a current total of 130 families in the CAZY classification,[1] which groups them based on amino acid sequence similarity. The vast majority of these enzymes conduct hydrolysis with either retention or inversion of anomeric configuration and proceed through oxocarbenium ion-like transition states. However, enzymes from families GH4 and GH109 employ an entirely different mechanistic strategy involving transient redox catalysis from a tightly bound NAD^+ cofactor and anionic transition states.[a] Detailed mechanistic studies by Yip et al.[2−5] in conjunction with several structural studies revealed the complex mechanism shown in Figure 1 that employs the following steps: (1) NAD^+-mediated oxidation of the C3 hydroxyl, (2) deprotonation at the substrate C2 position, (3) cleavage of the C1−O1 linkage via elimination across the C1−C2 bond, (4) 1,4-Michael-like addition of water at C1, (5) reprotonation at C2, and finally (6) reduction of the C3 carbonyl by the on-board NADH cofactor.[2,3,5,6] Through a combination of kinetic isotope effect measurements on substrates deuterated (individually) at C1, C2, and C3, along with Brönsted analyses using substrates bearing a range of aglycones of different leaving group abilities, the authors concluded that steps 1 and 2 (oxidation of C3 and deprotonation at C2) were both partially rate-limiting and that the elimination step itself was relatively rapid. These studies were performed on both an α-glycosidase (GlvA) and a β-glycosidase (BglT) from GH4. This conclusion was reinforced through a subsequent study by Bennet and co-workers on another GH4 α-glycosidase, MelA, which involved kinetic isotope effect measurements on a doubly deuterated substrate.[7]

The identities of the active site residues responsible for acid and base catalysis in these enzymes can be inferred from some of the structural studies, but definitive supportive evidence has not yet been provided through mechanistic studies with selected mutants. Indeed, the mutagenic studies reported to date were performed prior to the availability of crystal structures or the mechanistic elucidation, and as it turned out, the residues mutated were not located in the active site.[8−10] In the cases of both BglT, a 6-phospho-β-glucosidase from *Thermotoga maritima*, and GlvA, a 6-phospho-α-glucosidase from *Bacillus subtilis*, a tyrosine residue has been proposed to act as the catalytic base responsible for C2 deprotonation on the basis of its location in the X-ray crystal structure of an enzyme−product complex.[3,6,11] Furthermore, a pK_a value of 7 has been proposed for this Tyr residue based on the pH−activity profiles obtained for these two enzymes.[2,3,11] This Tyr residue is absolutely conserved among the 6-phosphoglycosidases in GH4. Interestingly, although there is no overall structural similarity between GH4 and GH109 enzymes, the active sites of BglT, GlvA, and an *N*-acetylgalactosaminidase from GH109 overlap well.[12] In particular, the NAD^+ cofactor, the substrate, and the proposed catalytic tyrosine base are found in the same arrangement in both families of enzymes.

This study concerns a mechanistic analysis of mutants of BglT, a well-studied retaining GH4 glycosidase in which the proposed catalytic base, Tyr 241, is replaced with Phe and Ala. A combination of pH profile, kinetic isotope effect studies, and pre-steady-state measurements provides strong support for this

Received: July 29, 2012
Revised: September 30, 2012
Published: October 1, 2012

dx.doi.org/10.1021/bi301021u | *Biochemistry* 2012, 51, 8464−8474

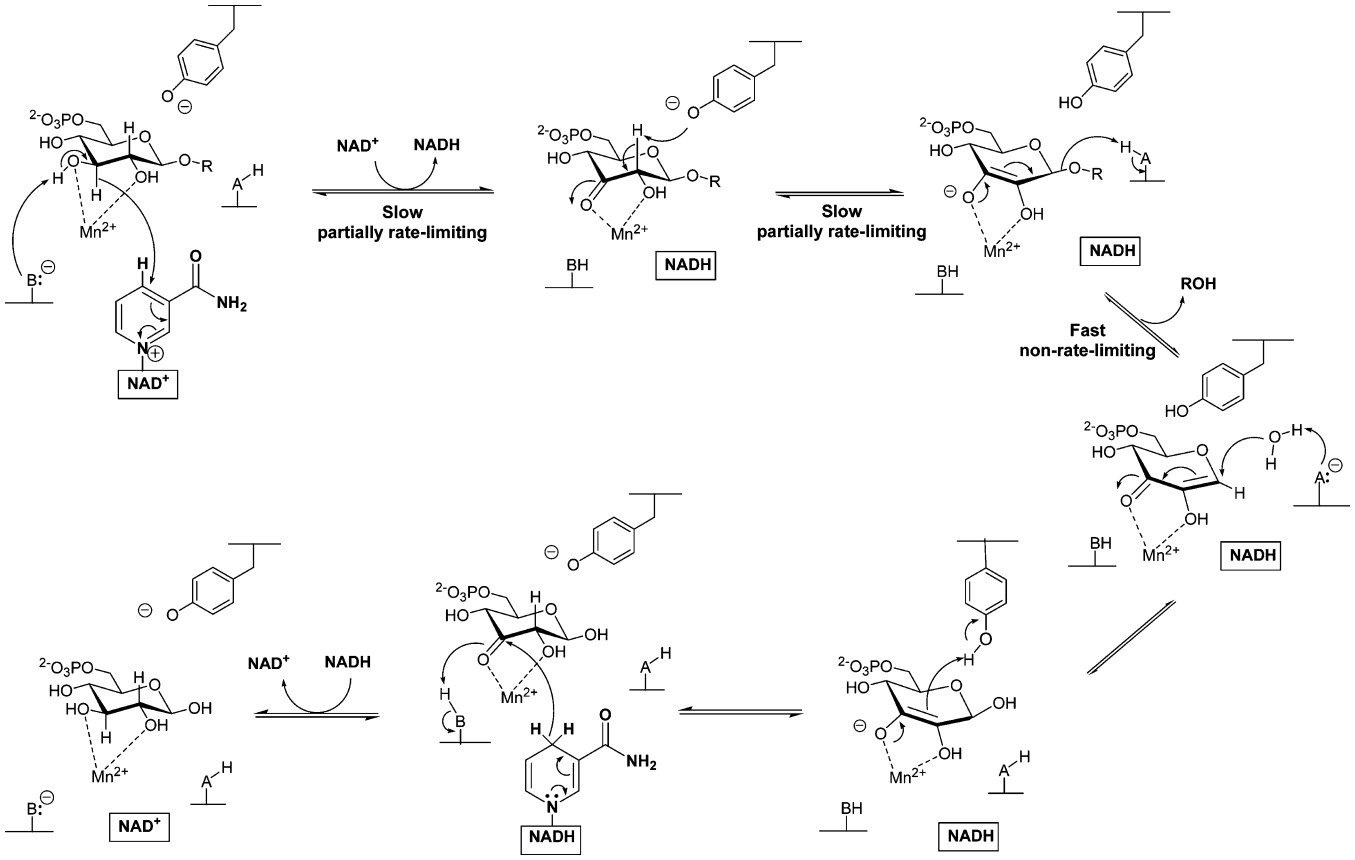

Figure 1. Proposed mechanism of BglT.

suggested role, thereby expanding the list of enzyme classes for which tyrosine residues have been shown to function as a base catalyst.

MATERIALS AND METHODS

General Methods. All NMR spectra were recorded at neutral pH on Bruker Avance 300 and Bruker Avance 400 spectrometers at 300 and 400 MHz, respectively. Chemical shifts are reported on the δ scale in parts per million from tetramethylsilane (TMS) and were referenced to D_2O. ^{31}P NMR signals were externally referenced to 85% H_3PO_4 in H_2O at 0 ppm. Low- and high-resolution mass spectra were collected by the mass spectrometry laboratory at the University of British Columbia. Elemental analyses were performed by M. Lakha of the microanalysis laboratory at the University of British Columbia.

Materials. All chemicals and reagents were purchased from Sigma-Aldrich unless stated otherwise. The kinase, BglK, was donated by J. Thompson.[13] All solvents were freshly distilled except where mentioned.

Synthesis of Aryl Glucosides. 4-Methylumbelliferyl 6-phospho-β-D-glucopyranoside was synthesized by the BglK-catalyzed phosphorylation of the commercially available 4-methylumbelliferyl β-D-glucopyranoside according to the procedure published by Thompson et al. with minor modifications.[13] The syntheses of all other aryl 6-phospho-β-D-glucopyranosides have been described previously.[5]

4-Methylumbelliferyl 6-Phospho-β-D-glucopyranoside Disodium Salt (4MUβG6P). ^1H NMR (300 MHz, D_2O): δ 7.58 (1 H, d, J = 8.8 Hz), 6.96 (1 H, dd, J = 8.8, 2.4 Hz), 6.95 (1 H, d, J = 2.4 Hz), 6.09 (1 H, s), 5.11−5.08 (1 H, m, H1), 3.98−3.84 (2 H, m, $H6_a$, $H6_b$), 3.60−3.50 (4 H, m, H2, H3, H4, H5), 2.28 (3 H, s, CH_3). ^{13}C NMR (75 MHz, D_2O): δ 164.68, 159.56, 156.35, 153.99, 126.86, 115.43, 113.87, 111.38, 103.72, 99.86 (C1), 75.89 (d, $J_{5,P}$ = 9.2 Hz, C5), 74.88, 73.10, 68.59, 62.40 (d, $J_{6,P}$ = 5.1 Hz, C6), 18.09 (CH_3). ^{31}P NMR (121 MHz, D_2O): δ 5.00 (1 P, t, $J_{6H,P}$ = 5.4 Hz). ESI-MS (high resolution): calcd for $[C_{16}H_{17}O_{11}Na_3P]^+$, m/z 485.0202; found, m/z 485.0203. Anal. Calcd for $C_{16}H_{17}O_{11}PNa_2{\cdot}4H_2O$: C, 35.97; H, 4.72. Found: C, 36.51; H, 4.64.

Enzyme Kinetics. All kinetic assays were conducted in 1 cm path length matched quartz cuvettes with a Cary 300 UV−vis spectrometer equipped with a circulating water bath, or a Cary 4000 UV−vis spectrometer with a Cary temperature controller attached. Unless stated otherwise, enzyme samples were preincubated in the assay buffer at 50 °C for 5 min prior to the addition of substrate to initiate the enzymatic reaction. All data fitting was performed with GraFit 4.0 or Cary WinUV, Kinetics Application, version 3.00 (182).

The following buffer systems were employed. Buffer A consisted of 50 mM HEPES, 0.1 mM $MnCl_2$, 1 μM NAD^+, 10 mM 2-mercaptoethanol, and 0.1% (w/v) BSA at pH 7.5. Buffer B consisted of 50 mM MES, 0.1 mM $MnCl_2$, 1 μM NAD^+, 10 mM 2-mercaptoethanol, and 0.1% (w/v) BSA at pH 6.5. Buffer C consisted of 50 mM Tris, 0.1 mM $MnCl_2$, 1 μM NAD^+, 10 mM 2-mercaptoethanol, and 0.1% (w/v) BSA at pH 8.0. Buffer D consisted of 50 mM Tris, 0.1 mM $MnCl_2$, 1 μM NAD^+, 10 mM 2-mercaptoethanol, and 0.1% (w/v) BSA at pH 8.4. Buffer E consisted of 50 mM Tris, 0.1 mM $MnCl_2$, 1 μM NAD^+, 10 mM 2-mercaptoethanol, and 0.1% (w/v) BSA at pH 9.0. Buffer F consisted of 50 mM CAPS, 0.1 mM $MnCl_2$, 1 μM NAD^+, 10 mM 2-mercaptoethanol, and 0.1% (w/v) BSA at pH 10.0.

dx.doi.org/10.1021/bi301021u | Biochemistry 2012, 51, 8464−8474

Conditions for Measurement of Initial Rates. The concentration of enzyme used for each substrate was chosen such that less than 10% of the total substrate was consumed, ensuring linear time courses. The enzyme was preincubated in the assay buffer mixture for 5 min, and the reaction was initiated by the addition of the appropriate substrate. The initial rate of hydrolysis was followed spectrophotometrically upon addition of the appropriate aryl 6-phospho-β-D-glucoside at the wavelength of maximal absorbance difference between the released phenol and the respective aryl 6-phospho-β-D-glucoside.

Conditions for the Substrate Depletion Method.[14] The k_{cat}/K_m analyses were performed by the depletion method using low substrate concentrations and by monitoring the change in absorbance at the wavelength of maximal absorbance difference between the released phenol and the respective aryl 6-phospho-β-D-glucoside over approximately 30 min until the reaction was complete. The data sets were fit to a first-order equation, and the k_{cat}/K_m values were obtained by dividing the pseudo-first-order rate constant obtained by the enzyme concentration.

Agarose (Bio-Rad, Hercules, CA) gel (1%) was used for all DNA electrophoreses. Sodium dodecyl sulfate−polyacrylamide gel electrophoresis (10% SDS−PAGE) (stained with Coomassie blue) was performed to analyze the homogeneity of proteins. The molecular weight markers used were a prestained SDS−PAGE standard (Bio-Rad). The following *Escherichia coli* strains were used: TOP10 for DNA isolation and BL21 for protein expression. Yeast extracts and Tryptone were purchased from Difco Laboratory. Acrylamide/*N*,*N*′-methylene bisacrylamide (40%) and *N*,*N*,*N*′,*N*′-tetramethylethylenediamine (TEMED) were purchased from Bio-Rad. For the study of BglT and BglT mutants, mass spectra were recorded using an ABI MDS-SCIEX API QSTAR Pulsar *i* mass spectrometer (Sciex, Thornhill, ON) at the University of British Columbia. Gene sequencing was performed by the Nucleic Acid Protein Service (NAPS) Unit at the University of British Columbia. Oligonucleotide primers were purchased from Integrated DNA Technologies.

The gene encoding the *T. maritima* 6-phospho-β-glucosidase (BglT) cloned into Pet22b (provided by G. Davies) was used as a template for the mutagenic polymerase chain reaction. A four-primer mutagenic strategy was devised to introduce the desired Tyr241Phe and Tyr241Ala mutations as follows.

Preparation of the pET22*bgltY241F* Clone. Two separate polymerase chain reactions were conducted to first generate two larger fragments of 700 bp each. For the first reaction, the forward primer used was T7_mut_fw (GTG ATG TCG GCG ATA TAG GCG CC) and the reverse flanking primer containing the mutation (in bold) was TM_BglT_Y241F_rev (G GTA GTA CCT CAG GAA AGG ATT CAC). In the second reaction, the forward primer contained the mutation TM_BglT_Y241F_fwd (GTG AAT CCT T**T**C CTG AGG TAC TAC C) and the reverse flanking primer was T7term (GCT AGT TAT TGC TCA GCG G). Two separate mixtures containing the Pet22b plasmid as a template and either set of the two primers just described were heated to 95 °C, after which the PCR was started by adding 5 units of *Pwo* DNA polymerase (Boehringer Mannheim). In a 50 μL final volume of PCR buffer [10 mM Tris-HCl (pH 8.85), 25 mM KCl, 5 mM $(NH_4)_2SO_4$, and 2 mM $MgSO_4$], genomic DNA (100 ng) was used as a template. *Pwo* DNA polymerase [2.5 units (Roche Applied Science)] was used as the enzyme. Twenty nanomoles of each dNTP and 50 pmol of each of the primers mentioned above were included. PCR cycles were performed in a thermal cycler (Perkin-Elmer, GeneAmp PCR System2400). The following program was used: denature template for 2 min at 94 °C and 20 cycles of 94 °C for 15 s, 55 °C for 30 s, and 72 °C for 1 min. Following agarose gel electrophoresis of the PCR mixtures, the two products were observed, one in each mixture. Both fragments were approximately 700 bp dsDNA when compared to a 100 bp dsDNA ladder. These two fragments were isolated using the Qiaquick PCR purification kit according to the manufacturer's protocol (Qiagen). The product from the reaction including primers T7_mut_fw was termed BglTY241F_fwd, and the product from the second reaction including T7term was named BglTY241F_rev. The *bgltY241F_fwd* and *bgltY241F_rev* gel-purified PCR fragments were used for a second PCR, containing the Pet22b plasmid as a template. The reaction mixture was heated to 95 °C, after which the PCR was started by adding 5 units of *Pwo* DNA polymerase (Boehringer Mannheim). Thirty PCR cycles (3 min at 94 °C, 30 s at 55 °C, and 60 s at 72 °C) were performed in a thermal cycler. The product of this reaction was purified and treated in the same manner as the *bgltY241F_fwd* and *bgltY241F_rev* fragments to yield *bgltY241F*, which was purified by agarose gel electrophoresis. The fragment was found to be approximately 1500 bp dsDNA when compared to a 100 bp dsDNA ladder. The *bgltY241F* fragment was cut with BamHI and NdeI and cloned into the original plasmid from which the insert had been removed using the same enzymes. Ligation of this BamHI and NdeI endonuclease-cut fragment with BamHI and NdeI endonuclease-cut pET22 was performed using T4 DNA ligase (1 unit/10 ng of DNA) at a ratio of 10:1 (insert:vector) at 25 °C. The product of the ligation reaction was transformed into chemically competent TOP10 cells. Host competent cells were mixed with the pET22*bgltY241F* plasmid. The mixture was kept on ice for 30 min and then transferred to a water bath at 42 °C for a heat shock for 1 min. The mixture was then quickly moved to ice for 1 min. The transformants were incubated in LB medium at 37 °C for 1 h and subsequently cultured on LB medium plates at 37 °C containing 100 μg/mL ampicillin. After an overnight incubation, several colonies were inoculated on the LB medium and cultured for 24 h at 37 °C. Cultured cells were centrifuged at 10000 rpm and 4 °C for 10 min, and DNA was isolated via the minipreparation technique. The sequence of the gene was confirmed by automated DNA sequencing performed by the NAPS unit.

Preparation of the pET22*bgltY241A* Clone. The *bgltY241A* gene was cloned exactly as described for BglT_Y241F except for the primers used. The reverse flanking primer containing the mutation in bold was TM_BglT_Y241A_rev (G GTA GTA CCT CAG GCC AGG ATT CAC) and the forward primer containing the mutation in bold TM_BglT_Y241A_fwd (GTG AAT CCT **G**GC CTG AGG TAC TAC C).

Expression and Purification of BglT WT and Mutants. The plasmid containing the *T. maritima* genomic DNA cloned into the Pet22b vector generously provided by G. Davies was transformed into electrocompetent BL21 cells. The cells were grown in Luria broth medium supplemented with 100 μg/mL ampicillin (LB_{Amp}). For expression of the *bglt* gene and mutants, cells were grown in Luria broth medium supplemented with 100 μg/mL ampicillin at 37 °C to an OD_{600} of approximately 0.6 before being induced with 0.1 mM IPTG. Overnight cultures were harvested by centrifugation (10 min at

5000 rpm), and the pellet from 1 L of culture was resuspended in 40 mL of 50 mM HEPES (pH 8.0). The cells were lysed with a French cell press. The cells were centrifuged for 30 min at room temperature and 18000 rpm to remove cell debris and intact cells. The supernatant was collected and incubated for 30 min at 70 °C to denature the non-thermally stable *E. coli* proteins. After centrifugation at 18000 rpm for 30 min, the clarified supernatant was recovered and loaded on a 5 mL HiTrap DEAE FF ion exchange column (Amersham). The column was washed with 10 volumes of 50 mM HEPES (pH 8.0) before the protein was eluted with a step gradient involving increasing concentrations of 50 mM HEPES containing 500 mM NaCl (pH 8.0). Protein purity was assessed by SDS–PAGE (10% gel). Fractions containing BglT were pooled and concentrated. The concentration of the protein sample was determined using the calculated extinction coefficient of 31410 M^{-1} cm^{-1} at 280 nm.

The BglT Y241A and -F mutants were expressed and purified as described above. Electrospray ionization mass spectrometry (ESI-MS) was also performed and was used to confirm the molecular weights of the mutants.

CD Spectroscopy. CD spectra were recorded on a Jasco J810CD spectropolarimeter at the Shared Spectroscopy and Kinetics Hub of the University of British Columbia Laboratory of Molecular Biophysics. The enzyme samples (BglT WT, BglT Y241A, and BglT Y241F) were prepared in 500 μL of 10 mM HEPES, 0.1 mM Mn^{2+}, 1 μM NAD^+, and 10 mM 2-mercaptoethanol (pH 7.5) at an enzyme concentration of 4 μg/mL. Sample readings were collected at 50 °C in 1 mm path length quartz cuvettes.

Michaelis–Menten Kinetic Parameters. A standard curve of 7-hydroxy-4-methylcoumarin at various concentrations (absorption maximum at 360 nm and emission maximum at 450 nm) in 1 M NaOH was generated and used to correlate the fluorescence intensity to the rate of hydrolysis.

BglT WT was incubated with various concentrations of 4MUβG6P (30–900 μM) under the standard assay conditions in buffer A at 50 °C; 20 μL aliquots were removed every minute for 5 min and quenched with 980 μL of 1 M NaOH, and the fluorescence was measured to determine the initial rates of hydrolysis. Hydrolysis of 4MUβG6P was also assayed via the direct UV–vis assay as described by Yip et al.,[5] monitoring at 365 nm ($\Delta\varepsilon$ = 4847 cm^{-1} M^{-1}) for the release of the 7-hydroxy-4-methylcoumarin.

BglT Y241F activity was assayed at 50 °C in buffer A via the direct UV–vis assay using 4NPβG6P as described for BglT WT.[3] BglT Y241A activity was assayed at 50 °C in buffer E via the direct UV–vis assay using 4NPβG6P as described for BglT WT. The stopped assay was also utilized with this mutant to confirm the kinetic parameters because the activity is significantly lower, making rate measurements by the direct UV–vis assay challenging. BglT Y241A was incubated with various concentrations of 4MUβG6P (30–900 μM) under the standard assay conditions in buffer E at 50 °C; 20 μL aliquots were removed every minute for 5 min and quenched with 980 μL of 1 M NaOH, and the fluorescence was measured to determine the initial rates of hydrolysis. In each case, the enzyme concentration was chosen such that less than 10% of the total substrate was consumed, ensuring linear rates.

Determination of the K_d Value for Mn^{2+}. The divalent metal ion binding properties of BglT Y241F and BglT Y241A were investigated in a manner similar to that described previously for the WT enzyme.[3] BglT Y241F and BglT Y241A were dialyzed against 5 × 3 L of 50 mM HEPES (pH 7.5) to remove any bound divalent metals prior to manipulation. Samples of dialyzed enzyme samples and Mn^{2+} were preincubated in buffer [50 mM HEPES (pH 7.5) for BglT Y241F and 50 mM Tris (pH 9.0) for BglT Y241A], 1 μM NAD^+, 10 mM 2-mercaptoethanol, and 0.1% (w/v) BSA at 50 °C for 5 min. 4NPβG6P (final concentration of >10K_m) was then added to the reaction mixture to give a final volume of 200 μL, and initial rates were measured. The reaction rate was plotted versus the concentration of Mn^{2+} to generate ligand binding curves using GraFit 4.[15]

Determination of the K_d Value for NAD^+. Determinations of the K_d values of NAD^+ for BglT Y241F and BglT Y241A were conducted as described previously for BglT WT.[5] BglT Y241F and BglT Y241A were dialyzed against 5 × 3 L of 50 mM HEPES (pH 7.5) to remove any bound cofactors prior to manipulation. Samples of dialyzed enzyme samples and NAD^+ were preincubated in buffer [50 mM HEPES (pH 7.5) for BglT Y241F and 50 mM Tris (pH 9.0) for BglT Y241A], 0.1 mM Mn^{2+}, 10 mM 2-mercaptoethanol, and 0.1% (w/v) BSA at 50 °C for 5 min. 4NPβG6P (final concentration of >10K_m) was then added to the reaction mixture to give a final volume of 200 μL, and initial rates were measured. The reaction rate was plotted versus the concentration of NAD^+ to generate a ligand binding curve for BglT Y241F using GraFit 4.[15] No ligand binding curve was generated for BglT Y241A.

Steady-State Accumulation of NADH. Cellobiose 6′-phosphate (C6′P) was synthesized as described by Thompson and co-workers.[13] BglT Y241A (6.1 μM) was incubated at 50 °C in 200 μL of buffer A. The UV–vis absorbance at 340 nm was monitored to detect the formation of NADH. At 10 min, C6′P was added to initiate the enzymatic reaction. The molar extinction coefficient of 6220 M^{-1} cm^{-1} ($\Delta\varepsilon$ of NADH) was used for the calculation of NADH concentrations.

Kinetic Isotope Effect Determination. The $(k_{cat})_H/(k_{cat})_D$ measurements were performed using [1-^{2}H]4NPβG6P, [2-^{2}H]4NPβG6P, and [3-^{2}H]4NPβG6P as described previously for BglT WT.[5] The kinetic isotope effects (KIEs) in this study were measured under three different pH conditions, at 1 pH unit below pH_{opt}, at pH_{opt}, and at 1 pH unit above pH_{opt}. KIEs for BglT WT were measured in buffers A, B, and D; KIEs for BglT Y241F were measured in buffers A, B, and D, and KIEs for BglT Y241A were measured in buffers C, E, and F. In each case, the enzyme was incubated in the appropriate buffer system, and the final concentration was chosen such that <10% of the 4NPβG6P was hydrolyzed. In each case, a concentration of substrate equivalent to 10 times its K_m value was used in an assay volume of 1 mL. Each measurement was repeated at least six times in alternation, and the $(k_{cat})_H/(k_{cat})_D$ value was calculated by dividing the rate constant for the protio substrate by the rate constant for the deuterio substrate.

pH–Activity Profile. The pH–activity profiles of the mutants were measured essentially as described previously or the wild-type enzyme.[5,11] The pH dependence of k_{cat}/K_m for BglT Y241F was therefore measured by the substrate depletion method at low concentrations of 4NPβG6P.[14] The pH dependence of k_{cat} was obtained by measuring the initial rates of hydrolysis of 4NPβG6P under saturating substrate concentrations. For BglT Y241A, the stopped fluorimetric assay was used to measure the initial rates of hydrolysis of 4MUβG6P (saturating substrate concentrations), yielding values of k_{cat} when the observed rate was divided by the enzyme concentration. BglT Y241A was incubated with the

dx.doi.org/10.1021/bi301021u | *Biochemistry* 2012, 51, 8464–8474

substrate under various pH conditions at 50 °C in 50 mM NaCl, 1 mM $MnCl_2$, 0.1 mM NAD^+, 10 mM 2-mercaptoethanol, and 0.1% (w/v) BSA containing the appropriate buffer system: 20 mM AcOH/NaOAc (pH 4.0–4.5), 20 mM MES (pH 6.1–6.7), 20 mM HEPES (pH 6.5–8.2), 20 mM Tris (pH 8.4–9.0), or 20 mM CAPS (pH 9.5–11.0). The low activity of BglT Y241A limited the use of the substrate depletion method; thus, only the pH dependence of k_{cat} was measured for this mutant.

Kinetic and Spectroscopic Investigation of Cofactor Reduction. The kinetic and spectroscopic investigation of the nicotinamide cofactor reduction was accomplished by the method described previously.[3] Samples of the mutants, BglT Y241F and BglT Y241A, were dialyzed prior to manipulation.

BglT Y241F and NAD^+ (final concentration of 10 μM) were preincubated in buffer A for 5 min, and then 4NPG6P was added to the reaction mixture (final volume of 200 μL) to initiate the enzymatic reaction. In a second reaction, dialyzed BglT Y241F, NAD^+ (final concentration of 10 μM), and $NaBH_4$ (final concentration of 10 mM) were preincubated in buffer A for 5 min, and 4NPG6P (final concentration of >10K_m) was added to a final assay volume of 200 μL. The change in A_{400} was monitored for 10 min prior to the addition of 10 μL of 200 μM NAD^+ to rescue enzyme activity. The change in A_{400} was then measured for an additional 10 min. The same experiment was performed for a sample of dialyzed BglT Y241A in buffer E.

In an experiment analogous to that performed for the wild-type (WT) enzyme,[5] the absorbance spectra (from 250 to 400 nm) of BglT Y241F at pH 7.5 were recorded under three conditions: 10 μM BglT Y241F, 10 μM BglT Y241F incubated with 10 μM NAD^+, and 10 μM BglT Y241F incubated with 10 μM NAD^+ and 10 mM sodium borohydride.

The absorbance spectra (from 250 to 400 nm) of BglT Y241A at pH 9.0 were recorded under three conditions: 10 μM BglT Y241A, 10 μM BglT Y241A incubated with 10 μM NAD^+, and 10 μM BglT Y241A incubated with 10 μM NAD^+ and 10 mM sodium borohydride.

RESULTS

CD Spectroscopy. CD spectra of BglT WT, BglT Y241F, and BglT Y241A were recorded and are shown in Figure 2. There is no significant difference between the CD spectra of the three enzymes, indicating that mutation of the active site Tyr did not affect overall protein folding.

Michaelis–Menten Kinetic Parameters. All Michaelis–Menten kinetic parameters determined for BglT WT,[3] BglT Y241F, and BglT Y241A are summarized in Table 1. BglT Y241F and BglT Y241A are approximately 100- and 1000-fold less active than the wild-type enzyme, respectively. BglT Y241A has slightly higher k_{cat} and K_m values for the hydrolysis of 4MUβG6P than for 4NPβG6P, which is similar to the trend observed for BglT WT. Furthermore, the kinetic parameters for 4MUβG6P obtained from the stopped fluorimetric assays are similar to those obtained by UV–vis, indicating that the two assays produced reproducible data and could be used in subsequent kinetic analyses of BglT Y241A.

Kinetic and Spectroscopic Investigation of the Role of NAD^+. Upon dialysis, BglT Y241F was found to be completely inactive in the absence of NAD^+; full activity (measuring the hydrolysis of 4NPβG6P via the direct spectrophotometric assay) could be restored to the mutant in a saturable fashion by titration with NAD^+ (Figure 3). A K_d value of 383 nM (Table 2) was obtained on the basis of a direct fit of the data to a hyperbolic equation using GraFit 4.[15]

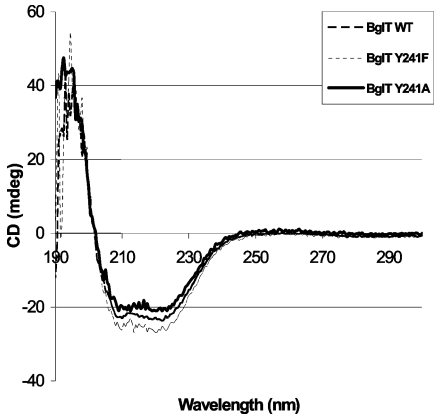

Figure 2. CD spectra of BglT WT, BglT Y241F, and BglT Y241A at 50 °C. Each spectrum was collected after the enzyme sample had been equilibrated at 50 °C for 20 min: (top line) BglT Y241A, (middle line) BglT WT, and (bottom) BglT Y241F.

The absorbance spectra (from 250 to 400 nm) of BglT Y241F were recorded under three different conditions: 10 μM BglT Y241F, 10 μM BglT Y241F incubated with 10 μM NAD^+, and 10 μM BglT Y241F incubated with 10 μM NAD^+ and 10 mM sodium borohydride. The peak in absorbance at 340 nm corresponding to NADH appears upon reduction with 10 mM sodium borohydride and is consistent with the quantitative reduction of NAD^+ to NADH (Figure 4a). On the basis of the small K_d value of 383 nM for NAD^+, more than 99% of BglT Y241F had NAD^+ or NADH bound to its active site under these conditions and very little remained free in solution. BglT Y241F activity was assayed in the presence of NAD^+, and the activity was compared to that obtained in the presence of NADH (quantitatively reduced from NAD^+ using sodium borohydride) as shown in Figure 4a. The enzyme was completely inactive in the presence of NADH (reduced form) alone. Upon addition of excess NAD^+ (after excess borohydride had been fully consumed by reaction with water), full activity (Figure 5a) was rapidly restored, demonstrating that the loss of activity upon reduction is due solely to having the dinucleotide cofactor in the wrong redox state as opposed to arising from protein denaturation or dramatic changes in pH.

Surprisingly, even after extensive dialysis, the NAD^+ remained tightly bound to BglT Y241A. Because the enzyme activity did not change with added NAD^+, a ligand binding curve could not be generated for this mutant. A final NAD^+ concentration of 10 μM was therefore included in all subsequent assays for the determination of Michaelis–Menten kinetics and KIEs, and this was assumed to provide saturating NAD^+ conditions. The absorbance spectra (from 250 to 400 nm) of BglT Y241A were recorded under two conditions: (i) 10 μM BglT Y241A and (ii) 10 μM BglT Y241A incubated with 10 mM sodium borohydride without added NAD^+ (Figure 4b). The peak in absorbance at 340 nm corresponding to NADH appeared upon reduction with 10 mM sodium borohydride, indicating that the tightly bound NAD^+ had been reduced to NADH. BglT Y241A activity was assayed in the presence of NAD^+, and the activity was compared to that obtained in the presence of NADH (quantitatively reduced from NAD^+ using sodium borohydride) as shown in Figure 5b. The mutant enzyme was completely inactive in the presence of

Table 1. Kinetic Parameters Determined for BglT WT, BglT Y241F, and BglT Y241A at 50 °C and pH 7.5 in Buffer A

	continuous UV assay, chromogenic substrate 4NPβG6P	relative to BglT WT	stopped fluorimetric assay, fluorogenic substrate 4MUβG6P	relative to BglT WT	continuous UV assay, fluorogenic substrate 4MUβG6P
			BglT WT		
k_{cat} (s^{-1})	0.99	1.0	1.0	1.0	1.2
K_m (μM)	48	1.0	94	1.0	83
k_{cat}/K_m (s^{-1} mM^{-1})	21	1.0	11	1.0	14
			BglT Y241F		
k_{cat} (s^{-1})	0.013	0.013	–	–	–
K_m (μM)	62	1.3	–	–	–
k_{cat}/K_m (s^{-1} mM^{-1})	0.21	0.010	–	–	–
			BglT Y241A		
k_{cat} (s^{-1})	9.6×10^{-4}	9.7×10^{-4}	1.1×10^{-3}	1.1×10^{-3}	–
K_m (μM)	134	2.8	289	3.1	–
k_{cat}/K_m (s^{-1} mM^{-1})	7.2×10^{-3}	3.4×10^{-4}	3.8×10^{-3}	3.5×10^{-4}	–

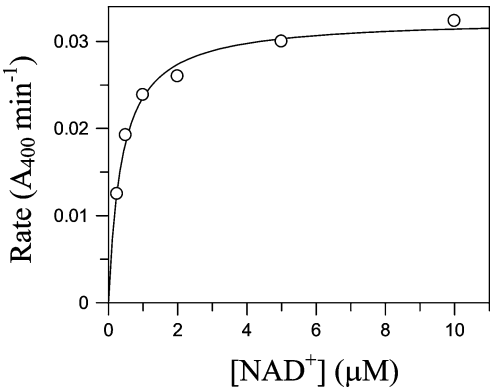

Figure 3. NAD^+ ligand binding curve obtained for BglT Y241F. Activity at each NAD^+ concentration was determined by UV–vis spectrometry using saturating 4NPβG6P as a substrate.

Table 2. Summary of Mn^{2+} and NAD^+ Dissociation Constants with BglT WT, BglT Y241F, and BglT Y241A

	K_d (μM) with Mn^{2+}	K_d (nM) with NAD^+
WT BglT	32	480
BglT Y241F	14	383
BglT Y241A	40	not available

NADH (reduced form) alone. Upon addition of excess NAD^+, full activity (Figure 5b) was rapidly restored, demonstrating that the loss of activity upon reduction is due solely to having the dinucleotide cofactor in the wrong redox state and showing that NAD^+–NADH exchange is possible, even though it cannot be removed by dialysis. These data suggest that BglT Y241F and BglT Y241A utilize the nicotinamide cofactor in a redox-dependent reaction step, as does the wild-type enzyme.

Determination of the K_d for Mn^{2+}. Similar to the WT enzyme, both mutants were completely inactive in the absence of Mn^{2+}, and full activity could be restored in a saturable fashion by titration with Mn^{2+}. The rates of hydrolysis of 4NPβG6P by BglT Y241F and BglT Y241A were measured at various concentrations of Mn^{2+}, and the data were fit to standard ligand binding curves (Figure 6). Dissociation constants were calculated and are listed in Table 2.

pH–Activity Profile. pH–activity profiles for BglT WT, BglT Y241F, and BglT Y241A were measured and are shown in Figure 7: the WT data have been scaled to fit on the same plots.

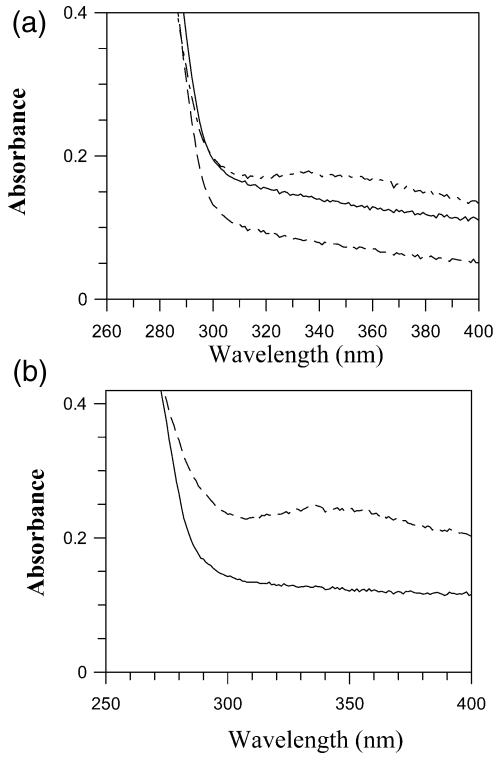

Figure 4. Absorbance spectra of BglT Y241F and BglT Y241A in their oxidized (NAD^+) and reduced (NADH) forms. (a) Absorbance spectra of 10 μM BglT Y241F (——, middle), 10 μM BglT Y241F incubated with 10 μM NAD^+ (– – –, bottom), and 10 μM BglT Y241F incubated with 10 μM NAD^+ and 10 mM sodium borohydride (–·–, top). (b) Absorbance spectra of 10 μM untreated BglT Y241A (—, bottom) and 10 μM BglT Y241A incubated with 10 mM sodium borohydride (– – –, top).

Each set of data was fit to classic bell-shaped curves, and the pK_{a1}, pK_{a2}, and pH_{opt} values are summarized in Table 3. For the mechanism in question, the acidic limb of the profile might be expected to reflect the catalytic base and differ between mutants in which the base residue is removed. The pH dependence of k_{cat}/K_m reflects ionizations in the free enzyme and free substrate; thus, because the substrate is the same in all cases, shifts in pK_a observed must reflect differences in active site residues. The pH dependence of k_{cat} reflects ionizations in the enzyme–substrate complex for the step that is rate-limiting;

dx.doi.org/10.1021/bi301021u | Biochemistry 2012, 51, 8464–8474

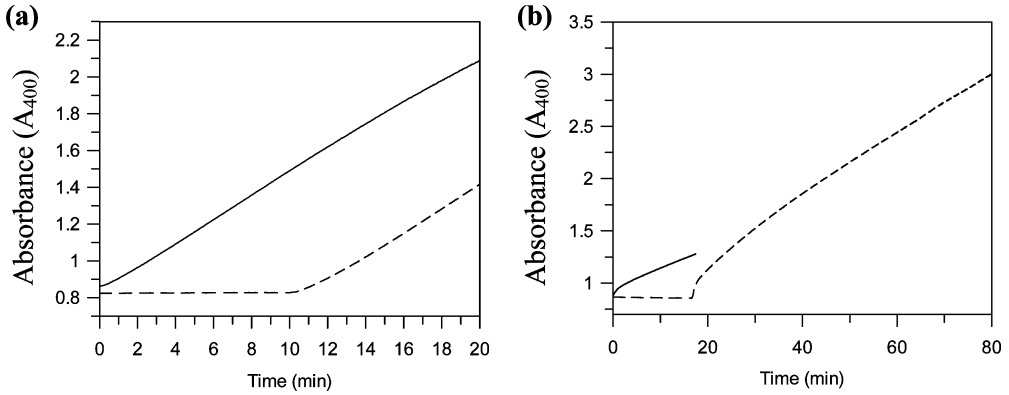

Figure 5. Assay of BglT mutants in the oxidized (NAD^+) and reduced (NADH) states. (a) Observed rates of hydrolysis of 4NPβG6P by BglT Y241F via the detection of 4-nitrophenolate release at 400 nm. Control (—): standard BglT Y241F assay conditions, 50 mM HEPES (pH 7.5), 0.1 mM $MnCl_2$, 10 μM NAD^+, 10 mM 2-mercaptoethanol, and 0.1% (w/v) BSA at 50 °C. BglT Y241F assay conditions (---): BglT Y241F preincubated in 50 mM HEPES (pH 7.5), 0.1 mM $MnCl_2$, 10 μM NAD^+, 10 mM $NaBH_4$, 10 mM 2-mercaptoethanol, and 0.1% (w/v) BSA at 50 °C. No release of 4-nitrophenolate was observed until 10 min, when 2 nmol of NAD^+ was added. (b) Observed rates of hydrolysis of 4NPβG6P by BglT Y241A via the detection of 4-nitrophenolate release at 400 nm. Control (—): standard BglT Y241A assay conditions, 50 mM HEPES (pH 7.5), 0.1 mM $MnCl_2$, 10 μM NAD^+, 10 mM 2-mercaptoethanol, and 0.1% (w/v) BSA at 50 °C. BglT Y241A assay conditions (---): BglT Y241A preincubated in 50 mM HEPES (pH 7.5), 0.1 mM $MnCl_2$, 10 μM NAD^+, 10 mM $NaBH_4$, 10 mM 2-mercaptoethanol, and 0.1% (w/v) BSA at 50 °C. No release of 4-nitrophenolate was observed until 18 min, when 2 nmol of NAD^+ was added.

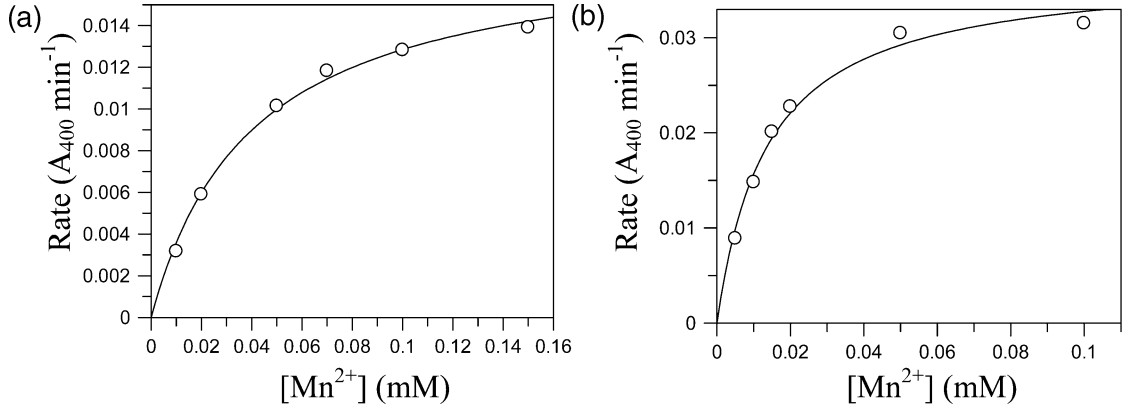

Figure 6. Titration of mutants with Mn^{2+}: (a) Y241A and (b) Y241F. Activity at each Mn^{2+} concentration was determined by UV−vis spectrometry using saturating 4NPβG6P as the substrate.

thus, its interpretation is much more complex, especially in cases such as this where the rate-determining step changes with pH, as revealed through measurement of KIEs at different pH values. The pH profile of k_{cat}/K_m for BglT Y241F reveals that only the acidic limb shifts, consistent with Y241 functioning as a base catalyst. Via SA, similar shifts in pK_{a1} were observed for BglT Y241F in the k_{cat} profile, but in this case, a shift of 1 pH unit was also measured for pK_{a2}. Further, in the k_{cat} profile of the BglT Y241A mutant, both pK_{a1} and pK_{a2} were shifted higher by more than 1 unit than that for BglT WT. These shifts in the pK_{a1} values for BglT Y241F and BglT Y241A are completely consistent with the removal of the active site Tyr base, with some other base-catalyzed process becoming rate-limiting, or with a different base fulfilling that role. Shifts in pK_{a2} in the k_{cat} profiles are more difficult to interpret because more than one step contributes, and the contribution of each step changes with pH, as noted below.

Steady-State Accumulation of NADH. Because the rate-limiting step for BglT Y241A appeared to be oxidation (vide infra), and because NAD^+ or NADH is tightly bound, it seemed probable that accumulation of on-board NADH might be observable during normal turnover. To probe this possibility, we incubated the mutant in the absence of substrate, and the UV−vis absorbance at 340 nm was monitored to detect the formation of NADH. At 10 min, the spectrophotometrically silent substrate cellobiose 6′-phosphate was added to the mixture, after which steady-state accumulation of NADH was observed as shown in Figure 8. The change in the absorbance indicated the presence of approximately 6 μM enzyme-bound NAD^+, which corresponds to the concentration of BglT Y241A used.

Kinetic Isotope Effects. KIEs were measured for BglT WT, BglT Y241F, and BglT Y241A at three different pH values: 1 pH unit below pH_{opt}, pH_{opt}, and 1 pH unit above pH_{opt}. All data are summarized in Table 4. The deuterium substitutions of interest were located at C1−C3 of the chromogenic substrate 4NPβG6P.

DISCUSSION

A number of attempts have been made previously to identify potentially important amino acid groups in GH4 enzymes through site-directed mutagenesis of conserved residues. The amino acid residues in question included those involved in binding the NAD^+ cofactor in the Rossman fold,[9] a strictly

dx.doi.org/10.1021/bi301021u | Biochemistry 2012, 51, 8464−8474

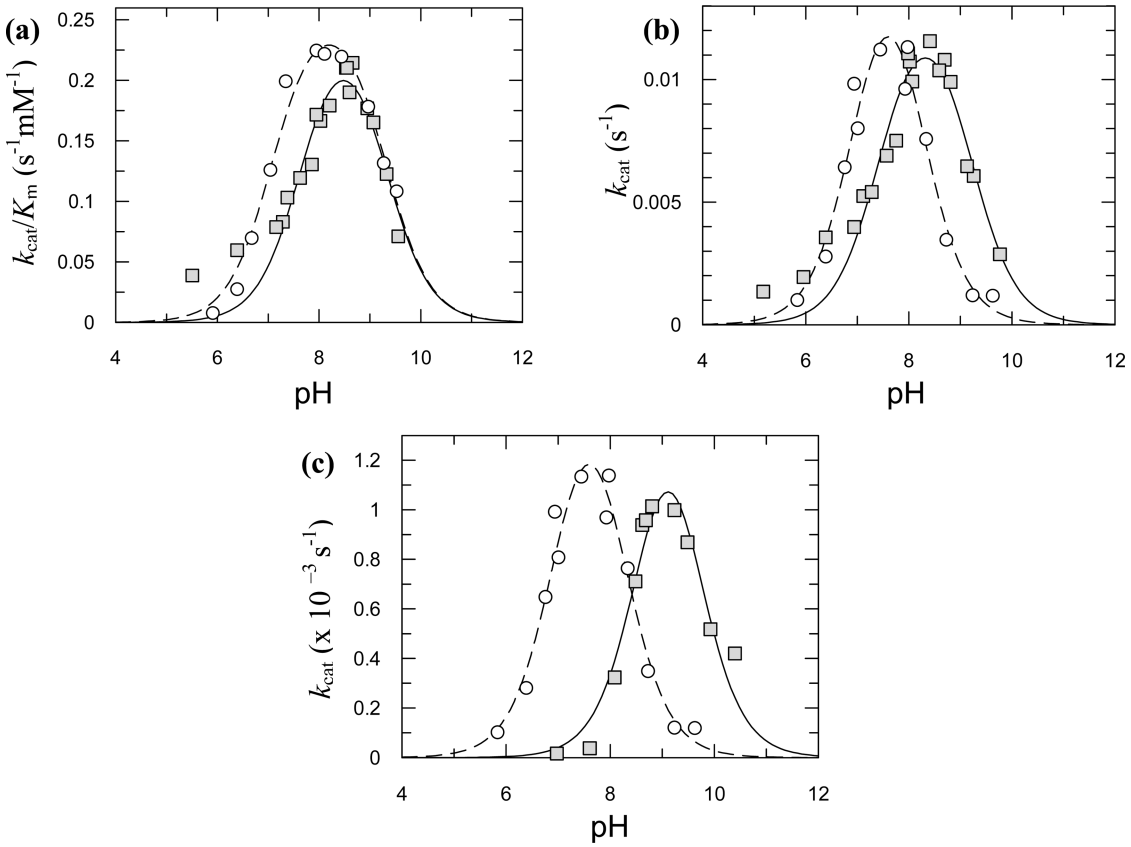

Figure 7. pH−activity profiles of BglT mutants. The gray squares represent the data of the mutant in each case, and the white circles represent the data obtained for BglT WT scaled to fit each plot: (a) k_{cat}/K_m vs pH for BglT Y241F, (b) k_{cat} vs pH for BglT Y241F, and (c) k_{cat} vs pH for BglT Y241A.

Table 3. Summary of Apparent pK_a and pH_{opt} Values for BglT WT, BglT Y241F, and BglT Y241A

	pH data based on k_{cat} or k_{cat}/K_m	pK_{a1}	pK_{a2}	pH_{opt}
BglT WT	k_{cat}	7.0 ± 0.1	8.2 ± 0.1	7.6
	k_{cat}/K_m	7.1 ± 0.1	9.3 ± 0.1	8.2
BglT Y241F	k_{cat}	7.4 ± 0.1	9.2 ± 0.1	8.3
	k_{cat}/K_m	7.7 ± 0.1	9.3 ± 0.1	8.5
BglT Y241A	k_{cat}	8.6 ± 0.2	9.6 ± 0.2	9.1
	k_{cat}/K_m	–	–	–

conserved Cys that is chelated to the divalent metal,[3,6,10] and an Asp residue adjacent to the active site Cys.[10] Identification of other catalytic residues was based largely on structural analyses. From the preliminary structural analyses, Asp260 has been proposed to act as the catalytic base for C2 deprotonation in AglA, an α-glucosidase from *T. maritima*, based on the available structure and the mechanism proposed for other GH4 members,[6,8,11] whereas a Tyr likely plays the same role in the 6-phosphoglycosidases (such as GlvA and BglT).[3,6,11] The preference for Tyr in the 6-phosphoglycosidases was suggested to be due to the need to circumvent the potential electrostatic repulsion between the C6 phosphate group of the substrate and

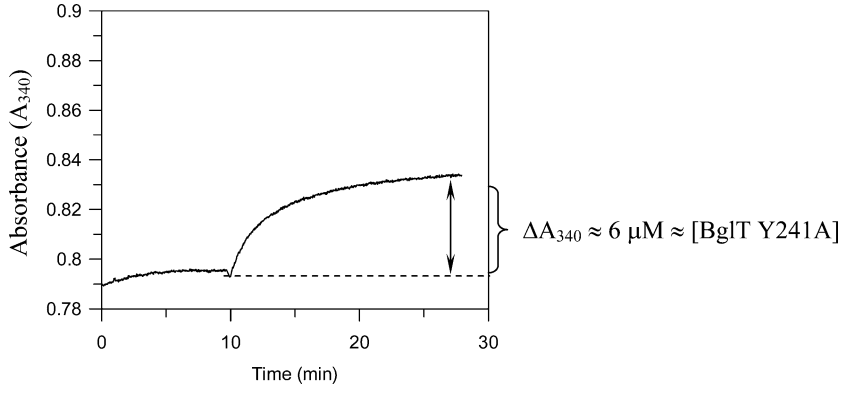

Figure 8. Steady-state accumulation of NADH during the BglT Y241A-catalyzed hydrolysis of C6′P. The absorbance of a sample of BglT Y241A is monitored at 340 nm. The reaction is initiated by the addition of C6′P at 10 min, at which point steady-state accumulation of NADH is observed.

dx.doi.org/10.1021/bi301021u | *Biochemistry* 2012, 51, 8464−8474

Table 4. KIEs Measured for BglT WT, BglT Y241F, and BglT Y241A

	pH 6.5 MES		pH 7.5 HEPES		pH 8.4 Tris	
substrate	$(k_{cat})_H/(k_{cat})_D$	KIE	$(k_{cat})_H/(k_{cat})_D$	KIE	$(k_{cat})_H/(k_{cat})_D$	KIE
			BglT WT			
[1-^{2}H]4NPβG6P	1.16 ± 0.02	secondary	1.00 ± 0.01	none	1.00 ± 0.01	none
[2-^{2}H]4NPβG6P	4.89 ± 0.05	primary	1.84 ± 0.02	primary	1.47 ± 0.03	primary
[3-^{2}H]4NPβG6P	1.85 ± 0.08	primary	1.63 ± 0.01	primary	1.61 ± 0.02	primary
			BglT Y241F			
[1-^{2}H]4NPβG6P	1.03 ± 0.03	none or secondary	1.00 ± 0.01	none	1.00 ± 0.01	none
[2-^{2}H]4NPβG6P	4.2 ± 0.2	primary	2.06 ± 0.03	primary	1.50 ± 0.01	primary
[3-^{2}H]4NPβG6P	1.49 ± 0.07	primary	1.72 ± 0.01	primary	1.66 ± 0.03	primary
	pH 8.0 Tris		pH 9.0 Tris		pH 10.0 CAPS	
substrate	$(k_{cat})_H/(k_{cat})_D$	KIE	$(k_{cat})_H/(k_{cat})_D$	KIE	$(k_{cat})_H/(k_{cat})_D$	KIE
			BglT Y241A			
[1-^{2}H]4NPβG6P	–	–	0.93 ± 0.02	inverse	–	–
[2-^{2}H]4NPβG6P	5.8 ± 0.5	primary	2.54 ± 0.07	primary	1.65 ± 0.08	primary
[3-^{2}H]4NPβG6P	1.18 ± 0.04	primary	1.04 ± 0.01	primary	1.05 ± 0.03	primary

an Asp residue.[6,11] Indeed, other glycosidases also seem to avoid electrostatic repulsions in similar manners, with sialidases and *trans*-sialidases employing a Tyr nucleophile instead of an Asp or Glu, presumably to minimize interactions with the substrate carboxylate functionality.[16,17] The role of the general acid involved in protonation of the departing aglycone oxygen has been assigned to an Asp (in GlvA) or a His (in AglA) residue. Interestingly, for BglT, which undergoes a *syn* elimination, the Tyr that is assigned the function of general base is positioned a mere 3.4 Å from the glycosidic oxygen. Therefore, this Tyr likely bears the dual role of general base in C2 deprotonation and general acid in assisting C1−O1 bond cleavage and/or formation. This may seem unlikely at first consideration, but the discrete $E1_{cb}$ mechanism makes this role attractive. Furthermore, the pH−activity profile of BglT revealed an important ionizable group with a pK_a value of ∼7, which could correspond to the Tyr residue.[5]

Site-directed mutagenesis of Tyr241 to either a Phe or Ala led to a 100- or 1000-fold decrease in reaction rate, respectively (Table 1), consistent with an important catalytic role for Tyr241. It is curious that replacement of the Tyr with Phe did not cause a more dramatic loss of activity. However, it is possible that the Phe, with the help of a nearby water molecule, might assume the same position as the phenolate of Tyr, with the water molecule then functioning as the catalytic base. Alternatively, for either mutant, the 6-phosphate group of the substrate could adopt the role of the base, as seen previously in an aldolase.[18] Both limbs of the pH−activity profiles of the mutants were found to be shifted to the right, with the largest shift (1.6 pH units) being seen in the BglT Y241A mutant. As noted earlier, interpretation of these shifts is only simple for the k_{cat}/K_m profile: the involvement of multiple rate-limiting steps whose contributions change with pH renders profiles of k_{cat} extremely complex. However, it is quite plausible that ionization of residues coordinating the NAD, the metal, or the phosphate could start to be reflected in these profiles at higher pH values. Overall, the findings are consistent with the assertion that the pK_{a1} of 7 observed in the profile of k_{cat}/K_m for the wild-type enzyme corresponds to the ionization of Tyr241.

While both mutants were found to require exogenous Mn^{2+} for activity, they appeared to behave differently with respect to the other cofactor, NAD^+. For BglT Y241F, the nicotinamide cofactor could be dialyzed out of the enzyme active site, rendering the mutant completely inactive. Activity could be restored in a saturable fashion as shown in Figure 3, implicating NAD^+ in its critical redox role in the proposed mechanism. On the other hand, BglT Y241A remained active despite exhaustive dialysis, and added NAD^+ did not enhance rates. However, both samples of BglT Y241F and BglT Y241A were completely inactive after being treated with sodium borohydride, and full activity was rapidly restored to both mutants upon addition of a fresh aliquot of NAD^+. It therefore seems surprising that exchange of NAD^+ with NADH can occur in BglT Y241A but that removal via dialysis is not possible. In any case, the requirement for the NAD^+ cofactor in its correct oxidized form for both mutants is thereby established (Figure 4).

Direct Observation of NADH Formation in BglT Y241A. It had not proved possible previously, using the wild-type enzyme, to directly detect the reduction of the "on-board" NAD^+ during catalysis, in part because the step in which the sugar is oxidized is at least partially rate-limiting. However, the very slow turnover of BglT Y241A, the lack of a KIE on the 3-deutero substrate indicating that oxidation is not rate-limiting, and the tight binding of the nucleotide afforded an opportunity for such direct detection. Indeed, by use of the spectrophotometrically silent cellobiose 6′-phosphate substrate and high enzyme concentrations with no additional NAD^+ added, a stoichiometric absorbance change was observed at 340 nm from the accumulation of endogenous NADH (Figure 8). This steady-state accumulation of a full equivalent of NADH in BglT Y241A indicates that a step subsequent to oxidation, likely the proton abstraction step, is slower in the mutant enzyme than in BglT WT.

Kinetic Isotope Effects. Inspection of the KIEs (Table 4) suggests that BglT Y241F utilizes a mechanism similar to that of BglT WT to catalyze the hydrolysis of 4NPβG6P. Primary KIEs are measured for [2-^{2}H]4NPβG6P and [3-^{2}H]4NPβG6P, and no secondary KIE is observed for [1-^{2}H]4NPβG6P. This suggests that the C3 hydride abstraction and the C2 deprotonation steps are partially rate-limiting followed by a rapid cleavage of the C1−O1 linkage consistent with an $E1_{cb}$ mechanism. Similar conclusions were reached in an elegant study of another GH4 enzyme, MelA, by Bennet in which KIE measurements using doubly deuterated (C2 and C3) substrates demonstrated that both steps are rate-limiting and reaction proceeds through a single, concerted transition state.[7] It is

dx.doi.org/10.1021/bi301021u | *Biochemistry* 2012, 51, 8464−8474

conceivable that an active site water molecule, or the substrate phosphate, replaces the role of the phenolate anion of Tyr as the catalytic base in C2 deprotonation, although it is surprising that the pH dependence was so similar if this is the case.

KIEs were measured for BglT Y241A under more basic conditions because its pH_{opt} of 9.1 is higher and the data suggest that the contributions of the individual steps of the mechanism may be different from that of BglT WT or Y241F. For BglT Y241A, a significantly larger primary KIE was measured for [2-^{2}H]4NPβG6P than for BglT WT (Table 4). Meanwhile, a very small primary KIE was measured for [3-^{2}H]4NPβG6P and an inverse KIE for [1-^{2}H]4NPβG6P. The very small primary KIE measured for [3-^{2}H]4NPβG6P and the large primary KIE determined for [2-^{2}H]4NPβG6P suggest that the activation barrier to C2 deprotonation has increased. This is consistent with the removal of the catalytic Tyr base, such that oxidation of the C3 hydroxyl is no longer a primary rate-determining step. The small inverse KIE measured for [1-^{2}H]4NPβG6P either arises from some kind of β-KIE on the deprotonation event at C2 or reflects the rehybridization of the C1 sp^2 carbon to an sp^3-hybridized center during the 1,4-Michael-like addition, which may be partially rate-limiting for BglT Y241A.

The effect of pH upon KIEs was also determined (Table 4). For BglT WT, the KIEs at pH 7.5 and 8.4 are similar. Primary KIEs were measured for [2-^{2}H]4NPβG6P and [3-^{2}H]-4NPβG6P, while no KIE was determined for [1-^{2}H]4NPβG6P. At pH 6.5, primary KIEs were still measured for [2-^{2}H]-4NPβG6P and [3-^{2}H]4NPβG6P, and kinetic analysis of [1-^{2}H]4NPβG6P revealed a secondary KIE. In particular, the primary KIE for [2-^{2}H]4NPβG6P increases with a decreasing pH. This is consistent with a change in the ionization of Tyr241, which needs to be deprotonated for C2 proton abstraction as the pH drops below the pK_a value of ~7. As the concentration of Tyr241 in its deprotonated form decreases under more acidic assay conditions, the C2 proton abstraction step becomes more rate-limiting. This may also affect the 1,4-Michael-like addition step, which could account for the secondary KIE determined for [1-^{2}H]4NPβG6P. Under acidic conditions, the addition step may become slower, because the catalytic base residue located around the substrate anomeric center may become protonated, making it unable to activate a water molecule for addition to the α,β-unsaturated or enediolate intermediate. Similar results were observed for BglT Y241F. Primary KIEs were observed for [2-^{2}H]4NPβG6P and [3-^{2}H]4NPβG6P under all three pH conditions, and a possible secondary KIE was measured for [1-^{2}H]4NPβG6P at pH 6.5. Again, the primary KIE for [2-^{2}H]4NPβG6P increases with increasingly acidic conditions for reasons similar to those provided for BglT WT. The KIEs for BglT Y241A were determined under three different pH conditions flanking its pH optimum (pH 8.0, 9.0, and 10.0), and a similar, yet more extreme, trend for [2-^{2}H]4NPβG6P is observed for this mutant, with C2 deprotonation contributing more to the rate-determining step. Because of the limited availability of [1-^{2}H]4NPβG6P, the KIE for this compound was not measured for BglT Y241A at pH values other than its optimum. As is seen with BglT WT and BglT Y241F, only minor variations in the small primary KIE are observed for [3-^{2}H]4NPβG6P. Most importantly, the KIEs measured for [2-^{2}H]4NPβG6P for the wild-type enzyme and both mutants show a strong dependence upon pH. The data suggest that C2 deprotonation is the most pH-sensitive step and that Tyr 241 plays a crucial role in C2 deprotonation in the wild-type enzyme.

CONCLUSIONS

All the data collected are consistent with Tyr241 acting as the general base responsible for C2 deprotonation. Mutation of Tyr241 led to significant decreases in catalytic activity in the two mutants, BglT Y241F and BglT Y241A, and substantial shifts in the pH dependence of catalysis, as expected. The observation of pH-dependent kinetic isotope effects for the 1-, 2-, and 3-deutero substrates, in particular a large primary kinetic isotope effect for the 2-deutero substrate with both mutants at low pH, is strongly supportive of this role. Because the initial oxidation step is fast relative to deprotonation in BglT Y241A, and because this mutant binds the nucleotide cofactor extremely tightly, a pre-steady-state phase involving the stoichiometric accumulation of the reduced cofactor "on enzyme" is observed.

The use of a Tyr residue as the catalytic base is not common, but the presence of a phosphate group at the C6 position may explain the predilection for a Tyr residue over an Asp or Glu to minimize electrostatic repulsion. In that regard, a tyrosine residue has been proposed to act as the catalytic base in a number of enzymes utilizing similar C−H deprotonation and elimination mechanisms. One example is alanine racemase that uses a tyrosine as one of its bases for deprotonation of the substrate α-carbon.[19] Most notably, it has been proposed that the chondroitin AC lyase,[20,21] whose substrate also contains a negatively charged moiety, uses a tyrosine as a catalytic base for α-proton abstraction: further, the same residue is thought to protonate the leaving group, much as could well occur here. Likewise, a tyrosine base is proposed for dehydratases such as *Salmonella enterica* serovar *typhimurium* dTDP-D-glucose 4,6-dehydratase RmlB.[22] Finally, the GH109 *N*-acetylgalactosaminidase,[12] which similarly utilizes a redox elimination mechanism for hydrolysis, also appears to use a Tyr residue for C2 deprotonation similar to what is seen in 6-phosphoglycosidases of GH4.

AUTHOR INFORMATION

Corresponding Author

*Telephone: (604) 822-3402. Fax: (604) 822-8869. E-mail: withers@chem.ubc.ca.

Funding

This work was supported by grants from the Natural Sciences and Engineering Research Council of Canada, the Protein Engineering Network of Centres of Excellence, and the Canadian Institutes of Health Research. V.L.Y.Y. was funded by the Natural Sciences and Engineering Research Council of Canada and the Michael Smith Foundation for Health Research. The Jasco J-810 spectrometer was provided through grants from the Canada Foundation for Innovation and the British Columbia Knowledge Development Fund to the Laboratory for Molecular Biophysics.

Notes

The authors declare no competing financial interest.

ABBREVIATIONS

GH4, glycoside hydrolase family 4; 4MUβG6P, 4-methylumbelliferyl 6-phospho-β-D-glucoside; NAD^+, β-nicotinamide adenine dinucleotide; NADH, β-nicotinamide adenine dinucleotide, reduced; [1-^{2}H]4NPβG6P, 4-nitrophenyl [1-^{2}H]-6-

phospho-β-D-glucoside; [2-^{2}H]4NPβG6P, 4-nitrophenyl [2-^{2}H]-6-phospho-β-D-glucoside; [3-^{2}H]4NPβG6P, 4-nitrophenyl [3-^{2}H]-6-phospho-β-D-glucoside; 4NPβG6P, 4-nitrophenyl 6-phospho-β-D-glucoside; C6′P, cellobiose 6′-phosphate; KIE, kinetic isotope effect; ESI-MS, electrospray ionization mass spectrometry; UV−vis, ultraviolet−visible; WT, wild-type.

■ ADDITIONAL NOTE

[a]The exceptions are found in families 4 and 109. Although family 39 also includes both α-L-iduronidases and β-D-xylosidases, the anomeric configuration of α-L- and β-D-glycosides is the same, with the differing α- and β-designations arising because of the nomenclature used for D- and L-sugars.

■ REFERENCES

(1) Cantarel, B. L., Coutinho, P. M., Rancurel, C., Bernard, T., Lombard, V., and Henrissat, B. (2008) The Carbohydrate-Active EnZymes database (CAZy): An expert resource for glycogenomics. *Nucleic Acids Res. 37*, D233−D238.

(2) Yip, V. L. Y., Thompson, J., and Withers, S. G. (2007) Mechanism of GlvA from *Bacillus subtilis*: A detailed kinetic analysis of a 6-phospho-α-glucosidase from glycoside hydrolase family 4. *Biochemistry 46*, 9840−9852.

(3) Yip, V. L. Y., Varrot, A., Davies, G. J., Rajan, S. S., Yang, X. J., Thompson, J., Anderson, W. F., and Withers, S. G. (2004) An unusual mechanism of glycoside hydrolysis involving redox and elimination steps by a family 4 β-glycosidase from *Thermotoga maritima*. *J. Am. Chem. Soc. 126*, 8354−8355.

(4) Yip, V. L. Y., and Withers, S. G. (2004) Nature's many mechanisms for the degradation of oligosaccharides. *Org. Biomol. Chem. 2*, 2707−2713.

(5) Yip, V. L. Y., and Withers, S. G. (2006) Mechanistic Analysis of the Unusual Redox-Elimination Sequence Employed by *Thermotoga maritima* BglT: A 6-Phospho-β-glucosidase from Glycoside Hydrolase Family 4. *Biochemistry 45*, 571−580.

(6) Rajan, S. S., Yang, X., Collart, F., Yip, V. L. Y., Withers, S. G., Varrot, A., Thompson, J., Davies, G. J., and Anderson, W. F. (2004) Novel catalytic mechanism of glycoside hydrolysis based on the structure of an NAD^+/Mn^{2+}-dependent phospho-α-glucosidase from *Bacillus subtilis*. *Structure 12*, 1619−1629.

(7) Chakladar, S., Cheng, L. D., Choi, M., Liu, J., and Bennet, A. J. (2011) Mechanistic Evaluation of MelA α-Galactosidase from *Citrobacter freundii*: A Family 4 Glycosyl Hydrolase in Which Oxidation Is Rate-Limiting. *Biochemistry 50*, 4298−4308.

(8) Lodge, J. A., Maier, T., Liebl, W., Hoffmann, V., and Strater, N. (2003) Crystal structure of *Thermotoga maritima* α-glucosidase AglA defines a new clan of NAD^+-dependent glycosidases. *J. Biol. Chem. 278*, 19151−19158.

(9) Raasch, C., Armbrecht, M., Streit, W., Hocker, B., Strater, N., and Liebl, W. (2002) Identification of residues important for NAD^+ binding by the *Thermotoga maritima* α-glucosidase AglA, a member of glycoside hydrolase family 4. *FEBS Lett. 517*, 267−271.

(10) Thompson, J., Hess, S., and Pikis, A. (2004) Genes *malh* and *pagl* of *Clostridium acetobutylicum* ATCC 824 encode NAD^+- and Mn^{2+}-dependent phospho-α-glucosidase(s). *J. Biol. Chem. 279*, 1553−1561.

(11) Varrot, A., Yip, V. L. Y., Li, Y., Rajan, S. S., Yang, X., Anderson, W. F., Thompson, J., Withers, S. G., and Davies, G. J. (2005) NAD^+ and Metal-ion Dependent Hydrolysis by Family 4 Glycosidases: Structural Insight into Specificity for Phospho-β-D-glucosides. *J. Mol. Biol. 346*, 423−435.

(12) Liu, Q. P., Sulzenbacher, G., Yuan, H., Bennet, E. P., Pietz, G., Saunders, K., Spence, J., Nudelman, E., Levery, S. B., White, T., Neveu, J. M., Lane, W. S., Bourne, Y., Olsson, M. L., Henrissat, B., and Clausen, H. (2007) Bacterial glycosidases for the production of universal red blood cells. *Nat. Biotechnol. 25*, 454−464.

(13) Thompson, J., Lichtenthaler, F. W., Peters, S., and Pikis, A. (2002) β-Glucoside Kinase (BglK) from *Klebsiella pneumoniae*. *J. Biol. Chem. 277*, 34310−34321.

(14) Joshi, M. D., Sidhu, G., Pot, I., Brayer, G. D., Withers, S. G., and McIntosh, L. P. (2000) Hydrogen bonding and catalysis: A novel explanation for how a single amino acid substitution can change the pH optimum of a glycosidase. *J. Mol. Biol. 299*, 255−279.

(15) *GraFit*, version 5.0 (2010) Erithacus Software Ltd., Surrey, U.K.

(16) Watts, A. G., Damager, I., Amaya, M. L., Buschiazzo, A., Alzari, P., Frasch, A. C., and Withers, S. G. (2003) *Trypanosoma cruzi trans*-sialidase operates through a covalent sialyl-enzyme intermediate: Tyrosine is the catalytic nucleophile. *J. Am. Chem. Soc. 125*, 7532−7533.

(17) Newstead, S., Watson, J. N., Knoll, T. L., Bennet, A. J., and Taylor, G. (2005) Structure and mechanism of action of an inverting mutant sialidase. *Biochemistry 44*, 9117−9122.

(18) St-Jean, M., and Sygusch, J. (2007) Stereospecific proton transfer by a mobile catalyst in mammalian fructose-1,6-bisphosphate aldolase. *J. Biol. Chem. 282*, 31028−31037.

(19) Sun, S. X., and Toney, M. D. (1999) Evidence for a two-base mechanism involving tyrosine-265 from arginine-219 mutants of alanine racemase. *Biochemistry 38*, 4058−4065.

(20) Rye, C. S., and Withers, S. G. (2002) Elucidation of the mechanism of polysaccharide cleavage by chondroitin AC lyase from *Flavobacterium heparinum*. *J. Am. Chem. Soc. 124*, 9756−9767.

(21) Garron, M. L., and Cygler, M. (2010) Structural and mechanistic classification of uronic acid-containing polysaccharide lyases. *Glycobiology 20*, 1547−1573.

(22) Allard, S. T. M., Giraud, M. F., Whitfield, C., Graninger, M., Messner, P., and Naismith, J. H. (2001) The crystal structure of dTDP-D-glucose 4,6-dehydratase (RmlB) from *Salmonella enterica* serovar *typhimurium*, the second enzyme in the dTDP-L-rhamnose pathway. *J. Mol. Biol. 307*, 283−295.